AGU PUBLICATIONS

JGR

Journal of Geophysical Research: Atmospheres

RESEARCH ARTICLE
10.1002/2016JD025357

**Key Points:**
- Urban heat island intensity is proportional to the physical size of the city
- Heatwaves in larger cities amplify urban heat island intensity
- Urban heat island pattern connected to local factors

**Correspondence to:**
P. Ramamurthy,
pramamurthy@ccny.cuny.edu

**Citation:**
Ramamurthy, P., and E. Bou-Zeid (2017), Heatwaves and urban heat islands: A comparative analysis of multiple cities, *J. Geophys. Res. Atmos.*, *122*, 168–178, doi:10.1002/2016JD025357.

Received 17 MAY 2016
Accepted 19 DEC 2016
Accepted article online 21 DEC 2016
Published online 10 JAN 2017



# Heatwaves and urban heat islands: A comparative analysis of multiple cities

**P. Ramamurthy[1,2] and E. Bou-Zeid[3]**

[1]Department of Mechanical Engineering, CUNY City College, New York, New York, USA, [2]NOAA-CREST Center, CUNY City College, New York, New York, USA, [3]Department of Civil and Environmental Engineering, Princeton University, Princeton, New Jersey, USA

**Abstract** The recent International Panel on Climate Change report predicts the highly urbanized Northeastern U.S. to be at high risk to heat waves. Since urban residents and infrastructure are known to be highly vulnerable to extreme heat, the goal of this paper is to understand the interaction between the synoptic-scale heat wave and the city-scale urban heat island (UHI) effects. The study also qualitatively analyzes the primary factors that contribute to UHIs by comparing their intensities in different cities with distinct geo-physical characteristics. Our results, generated by using the Weather Research and Forecasting model augmented with advanced urban surface parameterizations, confirm that the amplitude of UHI is related to the physical size of the city. However, the results suggest that cities of comparabale sizes might interact differently with heat waves: in New York City; Washington, DC; and Baltimore (but not in Philadelphia) the regular UHI was amplified more strongly during heat waves compared to smaller cities. The results also establish that the pattern of UHI in different cities, its variability, and its interaction with heat waves are inherently linked to dynamic factors.

## 1. Background

Urban heat island intensity (UHI) is a thermal index that accounts for the local amplification in air (or less commonly surface) temperature due to anthropogenic modification of the land surface and heat emissions. It is commonly utilized as an indicator to account for the degree of urbanization [*Cui and Shi*, 2012]. While UHI is explicitly linked to the physical characteristics of a city (total land cover and morphology), its magnitude and variability are a function of nonlinear interactions between multiple dynamic factors [*Oke*, 1982; *Arnfield*, 2003; *Kanda*, 2007], which include the following:

1. *Thermal storage*: Built materials (concrete, asphalt, and steel) that populate urban areas have high thermal inertia that allows them to store heat during the daytime, which is then released back to the atmosphere as sensible heat during nighttime [*Ramamurthy et al.*, 2014], thereby increasing the UHI.
2. *Evaporative cooling*: Built surfaces lack the capacity to store moisture, thereby diminishing evaporative cooling. This results in a larger fraction of the available energy being partitioned to sensible heat [*Sailor*, 2008].
3. *Advective cooling*: The thermal gradient between the hot urban surface and the relatively cooler rural surface gives rise to secondary circulations that have a moderating effect on the urban air temperature [*Haeger-Eugensson and Holmer*, 1999]; a comparable cooling effect can also be achieved under moderate to strong wind conditions.
4. *Anthropogenic heat*: Combustion of fossil fuels for space-heating, heat rejected by cooling equipment, and the heat released from vehicle exhaust will contribute to strengthening the UHI [*Taha*, 1997].
5. *Climatology*: Proximity to large water bodies will induce sea breeze circulations that have a moderating influence on the UHI (*Vahmani and Ban-Weiss* [2016]).

The combination of these factors is the primary driver that influences the magnitude and pattern of the UHI. While urban meteorologists are aware of these processes, they have lacked the necessary tools to examine their action and interaction closely. Most observational studies have focused on single cities or certain neighborhoods and have relied on traditional experimental techniques like ground-based towers and remote sensing instruments [*Grimmond et al.*, 2006]. The Joint Urban 2003 [*Allwine et al.*, 2002] and Basel Urban Boundary Layer Study are two such studies [*Rotach et al.*, 2005]. These experiments have advanced our understanding of urban dynamics and physical processes; nevertheless, their footprint is restricted to a single

neighborhood or city. Satellite-based remote sensing studies have been popular in understanding UHI effects [*Chen et al.*, 2006] and offer a rich spatial coverage. The commonly used satellites have a resolution of 250 m in the infrared spectrum. These studies are, however, limited by poor sampling rate, contamination due to cloud cover, and aerosol effects and are restricted to land surface temperature based UHI. More recently, regional-scale numerical models coupled to advanced urban land surface schemes have been used to study UHI effects [*Ramamurthy et al.*, 2015; *Gutiérrez et al.*, 2013]. Apart from high spatial and temporal resolutions, numerical models have representation for various urban-scale processes and output three-dimensional vector and scalar fields that provide much richer data to analyze the urban environment.

To comprehend and disentangle the impact of the factors described above, this study compares the UHI patterns in multiple cities that vary in size and background climatology, providing a qualitative assessment of the role played by these factors in exacerbating urban air temperature relative to surrounding rural areas, which is the central theme of our analysis. Most previous numerical investigations have used weather forecasting models to focus on a single city using or have analyzed outputs from coarse climate models (where urban surface physics tend to be poorly represented) to look at a large sample of cities without delving into the physical causes of observed differences in UHI. This study thus aims to fill a gap by considering a small number of cities in comparable climate zones and with comparable housing stock and using high-resolution atmospheric models with new-generation urban surface representations to elucidate the physical drivers of differences in the UHIs between different cities.

Another important part of our analysis centers on understanding the UHI response of these multiple cities to heat waves. Heatwaves in the future are expected to occur more frequently and increase in intensity due to global warming [*Meehl*, 2004]. This will significantly impact urban areas that are already subjected to elevated air temperatures [*Grimmond et al.*, 2010]. Recent research has shown that heat waves have the potential to amplify UHI [*Li and Bou-Zeid*, 2013; *Ramamurthy et al.*, 2015], which will bear adverse consequences to urban residents. A heat wave, unlike a UHI, is a mesoscale event that brings warm air from the upper atmosphere [*Black et al.*, 2004; *Xoplaki et al.*, 2003].

Here we utilize the Weather Research and Forecasting (WRF) model to simulate a 28 day period on 13 July to 9 August 2006 centered on the Northeastern United States that includes two heat wave episodes (16–18 July 2006 and 01–03 August 2006). The 2006 heat wave episode affected much of the North Eastern U.S. In New York nearly 140 fatalities were recorded and the average mortality rate increased by 8% [*Department of Health New York City (NYC)*, 2006]; the death count is one of the highest ever recorded from a natural disaster in the city. The heat wave episode was widely covered in the public sphere. While the analysis concerns two heat wave events, the findings pertain more generally to any other time period given similar heat wave synoptic conditions and not significant changes in the local dynamics and land surface properties generating the UHI.

The variability of the UHI and its interaction with heat waves are analyzed for four upper tier cities (New York; Philadelphia; Washington, DC; and Baltimore) and three lower tier cities (Bridgeport, Harrisburg, and Albany), the locations of which are depicted in Figure 1. The upper tier cities have higher population and population density and are centers of larger metropolitan areas. In contrast, the lower tier cities occupy a much smaller footprint. It should be noted that UHI in this article refers to air temperature based UHI.

## 2. Numerical Simulations and Model Validation

The WRF model (version 3.6) is used to simulate a 28 day period between 12 July and 9 August 2006. The simulations were conducted with an advanced urban canyon model, the Princeton Urban Canyon Model, which can represent subfacet level fluxes and includes advanced representations of hydrological processes [*Wang et al.*, 2013]. A mosaic-based approach is implemented to compute surface fluxes [*Li et al.*, 2013]. The mosaic approach is pertinent for urban modeling as the land use type in most urban areas is highly variable. For example, if the land use type for a grid cell is 39% high-intensity urban, 32% medium-intensity urban, and 29% green cover (which is obtained from the national land cover 2016 database (NLCD)), WRF-Model for Simulating Aerosol Interactions and Chemitry (MOSAIC) will solve for all three land use categories and will fractionally add the computed fluxes. In the default dominant-category approach, WRF will assume the land cover type as high intensity. The NLCD 2006 is the first to report wall to wall cover change. It has an

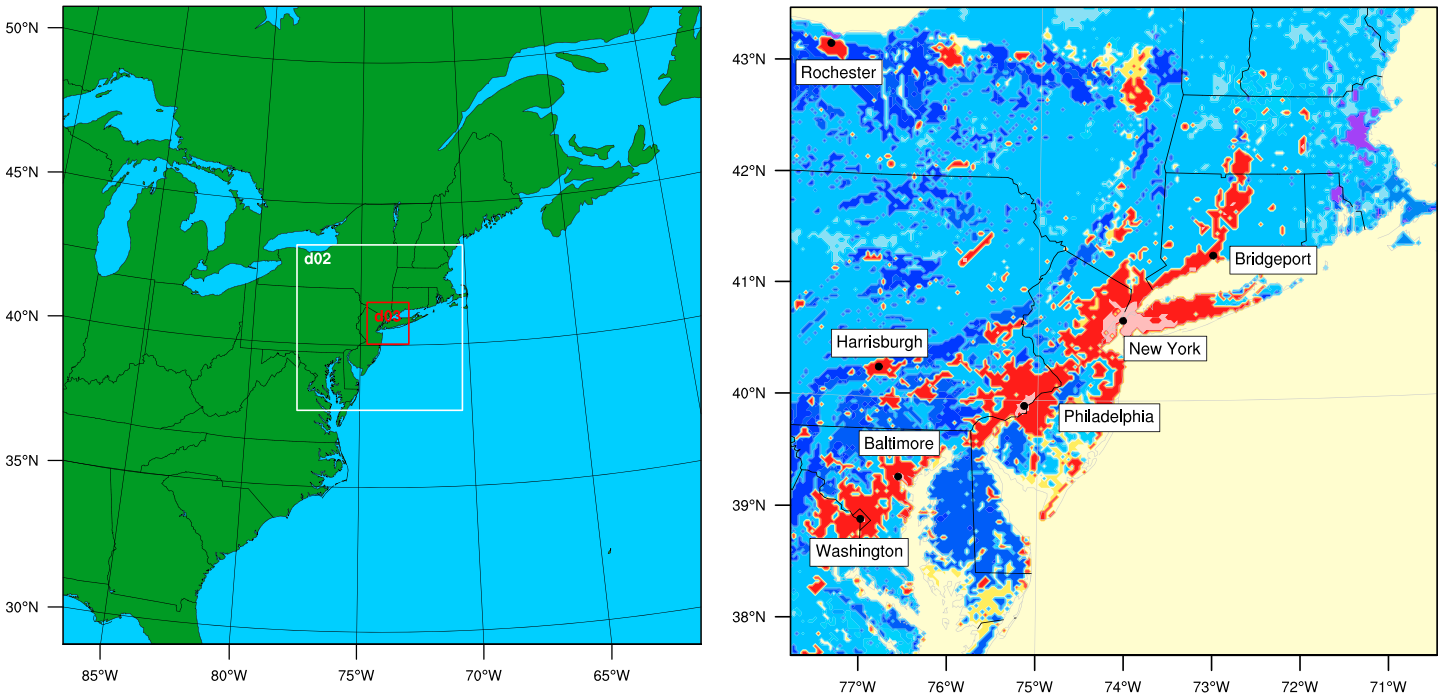


**Figure 1.** (left) The nested simulation domain. (right) The location of all the cities (red indicates urban land cover, and blue indicates crop and forest cover; yellow is water).

overall land cover accuracy of 76% and 80% for high-density urban [*Wickam et al.*, 2013]. These changes have improved the performance of our WRF simulation [*Li and Bou-Zeid*, 2014].

Three one-way nested domains with horizontal grid resolutions of 9, 3, and 1 km are used for the simulation, which is centered over New York City (Figure 1). For the analysis presented here, data from the 3 km domain is used (the 1 km domain was used for in-depth analyses of New York in *Ramamurthy et al.* [2015]). The simulation is driven by North American Regional Reanalysis data at 3 h intervals, and the NLCD 2006 land use categorization is used to determine the land use categories. The simulation used the rapid radiative transfer model scheme for longwave radiation [*Mlawer et al.*, 1997] and the Dudhia scheme [*Dudhia*, 1989] for shortwave radiation. The 2D Smagorinsky scheme is used for horizontal diffusion, and the mosaic-based Noah land surface model [*Li et al.*, 2013] is used for nonurban surfaces. The planetary boundary layer transport is parameterized by using the Mellor-Yamada-Janjic scheme [*Mellor and Yamada*, 1974] along with the modified Zilitinkevich relationship for thermal roughness length parameterization [*Chen and Zhang*, 2009]. Finally, the Princeton Urban Canopy Model (PUCM) with thermal surface properties calibrated for the Northeaster U.S. [*Wang et al.*, 2013] is used to represent urban surfaces. The NLCD 2006 has three urban categories: high, medium, and low intensities. The vegetated and built cover fraction and other aerodynamic properties for the three categories are derived from the WRF look-up table. The simulation was started on 12 July at 0000 UTC, and a 24 h warm up period was allowed before the data were collected for analysis.

The model was previously validated in *Li et al.* [2013] and *Ramamurthy et al.* [2015], but here we perform additional evaluation for this specific event and for various cities. Figure 2 compares land surface temperature observations from the simulation to that observed by the Moderate Resolution Imaging Spectroradiometer (MODIS) satellite. It also compares the 2 m air temperature derived from the simulation run to observations from the four large cities compared here. All the weather stations belong to the National Weather Service's Automatic Surface Observing System network. The comparison shows that the model performs well in replicating the actual conditions given the large spatial domain, the complex land surface characteristics, and the numerous parameterizations. The satellite image shows that the model does remarkably well in reproducing the urban rural gradient in surface temperature; a key factor is computing the UHI. The model performs equally well in reproducing the near surface air temperature during the heat wave episodes (square boxes in Figures 2c–2f). The root-mean-square error for Washington, Baltimore, Philadelphia, and New York City

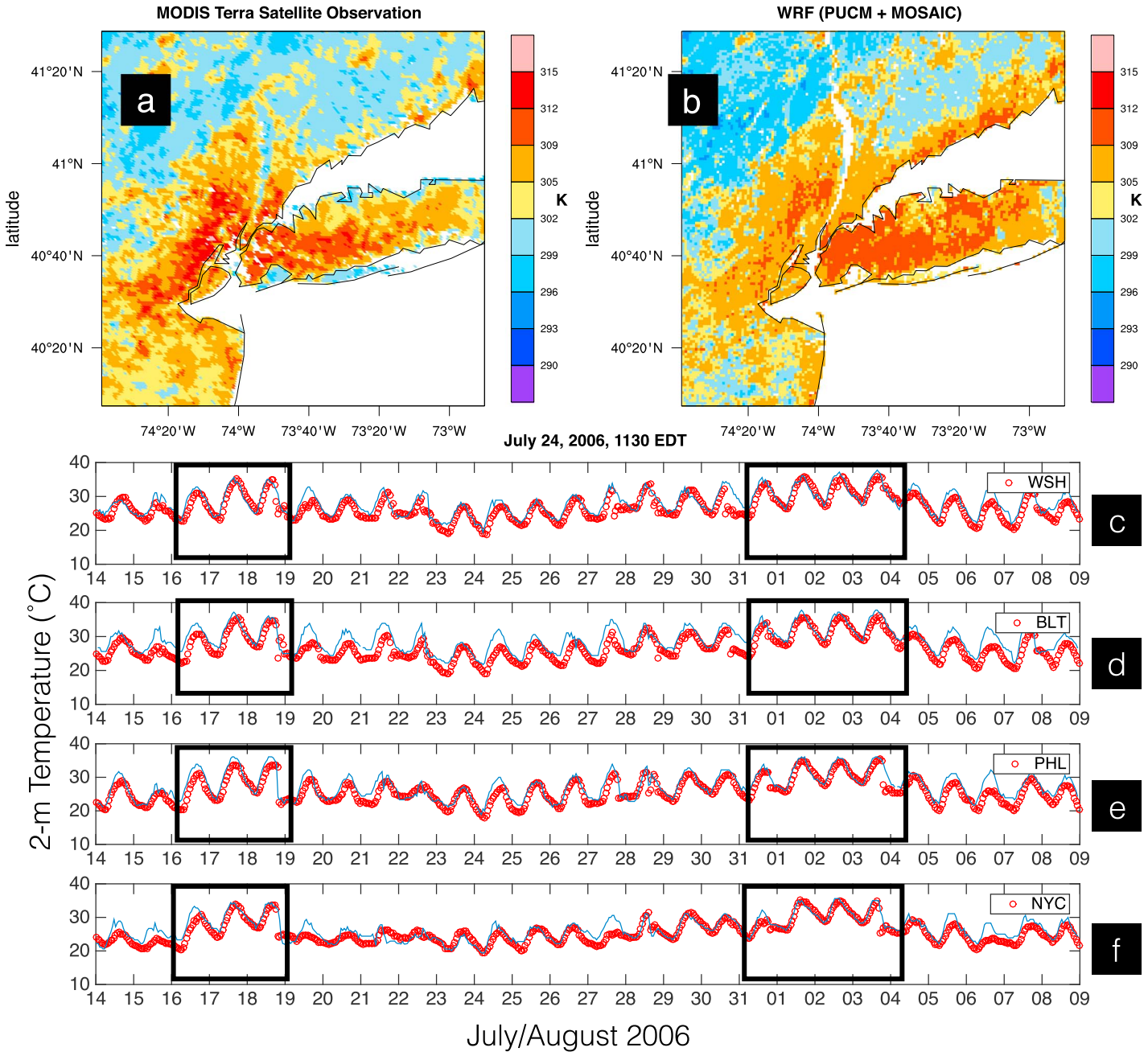


**Figure 2.** Comparing the performance of the model with observations. (a and b) Compare the land surface temperature from the model to a satellite image from MODIS. (c–f) Compare the 2 m air temperature to ground observations. The rectangular boxes indicate heat wave episodes.

are shown in Table 1 for different time periods. The values are much improved compared to previous studies [*Rosenzweig et al.*, 2009; *Meir et al.*, 2013]; this is directly attributable to the improved urban canyon and MOSAIC models.

For computing the UHI, the difference in 2 m air temperature between the urban and rural grid cells is used. From here on, UHI will only refer to air temperature-based UHI. The urban grid cells only include the dense city centers that are highly urbanized (dominated by high-intensity urban class), and hence, the results presented here can be interpreted as the spatially averaged maximum UHIs. The rural reference grid cells used did not contain any urban fraction and were dominated by vegetation, mostly broadleaf deciduous trees. In the case of New York and Philadelphia, the rural grid cells were 60 km and 30 km away from the city centers,

**Table 1.** Root-Mean-Square Error for Various Time Periods for Different Cities

| | Overall (°C) | Daytime (°C) | Nighttime (°C) | Heatwave (°C) |
|---|---|---|---|---|
| New York City | 2.06 | 2.39 | 1.58 | 1.92 |
| Philadelphia | 2.20 | 2.32 | 2.00 | 2.36 |
| Washington DC | 2.26 | 2.67 | 1.89 | 1.75 |
| Baltimore | 3.06 | 3.21 | 2.79 | 2.33 |

respectively, since both these cities were surrounded by large industrial and suburban spaces. The UHI computed from this analysis is compared to the average UHI observed by *Gedzelman et al.* [2003] in Figure 3. The researchers used data from nearly 75 weather stations in the New York Metropolitan area to study the mesoscale impact on UHI in New York City (NYC). Their study also addressed the seasonal and diurnal variability in UHI. The comparison between their average summer UHI with our modeled results shows a good agreement. It is remarkable that the diurnal cycles of the UHI between the model and observations match that well, despite the different conditions. WRF reproduces the high nighttime UHI, the low midday values, and the early morning and evening transition periods accurately. The model, however, overpredicts midday UHI by 0.75 K, which is potentially due to the discrepancies in spatially sampled data points and the comparison period.

## 3. Results and Discussion

### 3.1. UHI Pattern

The results reveal a consistent temporal trend in UHI in different cities, with high UHI observed during the nighttime (0030–0930 UTC, 2030–0530 local time), decreasing steadily after sunrise. The UHIs reach a minimum value of 0–1.5 K during the afternoon hours (Figure 4). The upper tier cities, however, experience higher UHI compared to lower tier cities. Maximum nighttime UHI for New York, Philadelphia, Washington, and Baltimore are 4.5 K, 4 K, 3.9 K, and 3.7 K, respectively. The maximum UHI in lower tier cities, on the other hand, average between 2 K and 2.5 K. This difference in UHI magnitude is also visible during the midday period; the UHI in upper and lower tier cities are around 1 K and 0–0.5 K, respectively. In the morning hours, the spatial uniformity of the incoming radiation results in more homogeneous surface temperatures and minimizes the difference between the urban and rural areas. The deeper convective boundary layer and enhanced mixing over the cities during daytime also aid in the effective transport of heat. These two factors aid in homogenizing the air temperature across the urban-rural divide. In the late evening and nighttime hours, on the other hand, the storage flux plays a crucial role in maximizing the UHI. Urban surfaces like concrete, asphalt, and

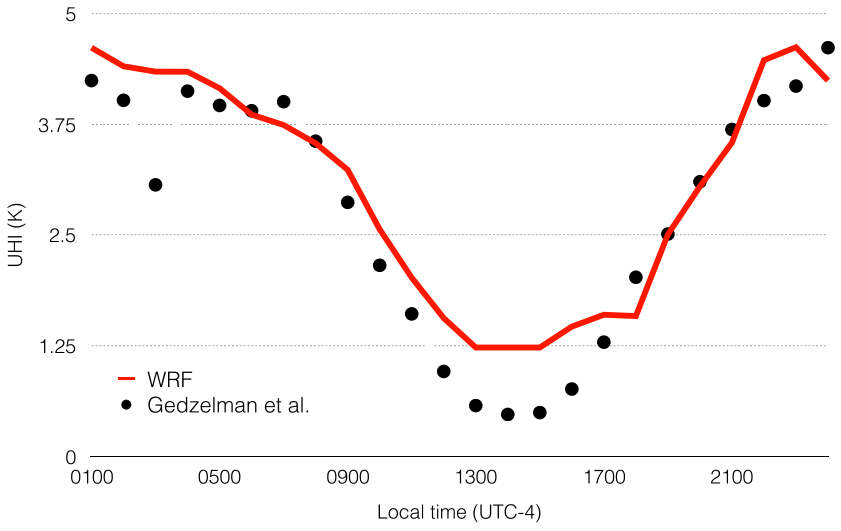


**Figure 3.** Comparing the average diurnal variability in UHI computed by the WRF model to that observed by *Gedzelman et al.* [2003].

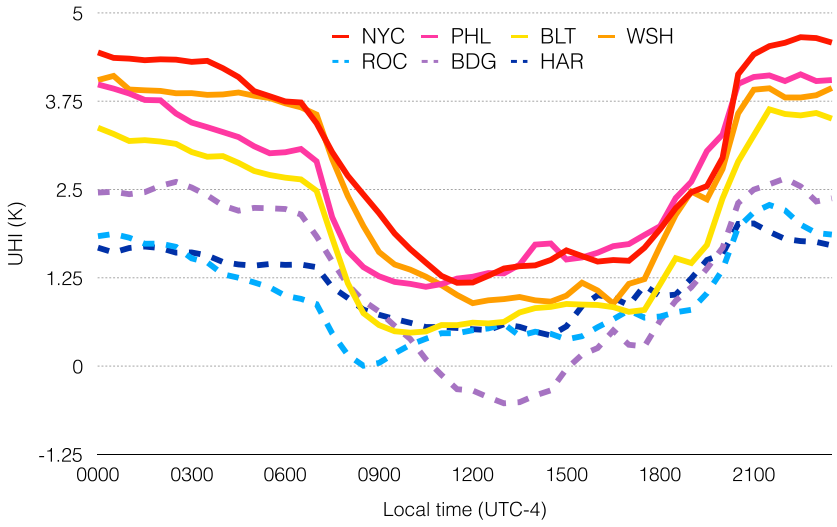


**Figure 4.** Diurnal variability of UHI averaged over the whole simulation period. The dashed lines indicate lower tier cities, and the solid lines denote upper tier cities. NYC, PHL, BLT, WSH, ROC, BDG, and HAR stand for New York City; Philadelphia; Baltimore; Washington, DC; Rochester; Bridgeport; and Harrisburg, respectively.

steel have high thermal inertia and retain significantly more thermal energy than vegetated terrain. The nighttime storage fluxes ($\Delta G$) that are released from the subsurface into the atmosphere for an urban grid cell are about 100 W m$^{-2}$ for lower tier cities and about 300 W m$^{-2}$ for upper tier ones, compared to 50–100 W m$^{-2}$ for rural surfaces. This stored heat dissipates as sensible heat, resulting in stronger surface temperature differences. This phenomenon makes urban areas a source of heat all through the night and, along with reduced turbulence and mixing, explains the stronger nighttime UHI.

The storage flux is a function of total built area but is sensitive to variability in incident weather, like changes in cloud cover and precipitation. Figure 5 compares the averaged diurnal variation in spatially aggregated storage heat flow for three different cities: New York, Philadelphia, and Harrisburg. The plot is obtained by integrating the storage heat flux over the entire city,

$$G = \iint \Delta G \; dxdy, \tag{1}$$

where $\Delta G$ is storage flux and $dx$ and $dy$ are the horizontal grid spacing. The storage flux shows similar diurnal trends at all three cities with positive peaks around 1700–1800 UTC (1300–1400 local time). However, there is appreciable disparity in the magnitude of $\Delta G$ and an even stronger disparity in its spatial integral $G$. It is interesting to note that while the average $\Delta G$ peak for New York is close to 300 W m$^{-2}$, Philadelphia and Rochester have peaks close to 180 and 100 W m$^{-2}$. This difference in $\Delta G$ is related to the difference in UHI: for larger cities, the air gets hotter and is less able to extract heat from the surface; a larger fraction of the net radiation flux must then go toward ground storage. The difference in $G$, however, is also related to the size of the city: NYC, which covers 790 km$^{-2}$, has an average peak value around 3.5 GW compared to 20 MW for Philadelphia and 4 kW for Harrisburg. The difference in magnitude is directly proportional to the area occupied by the cities, and this overwhelming disparity in storage heat flux is the primary factor that controls the daily pattern of UHI among cities. The stored heat is later (during nighttime) released as sensible heat flux back in to the atmosphere. The storage heat is mainly responsible for maintaining high nighttime temperatures in urban areas. *Ramamurthy et al.* [2014] showed that concrete, which has high heat capacity, plays a central role in maintaining urban areas as a heat source during the nocturnal period. In stark contrast, rural surfaces lack the capacity to retain heat. This redistribution mechanism helps maintain urban areas warmer compared to the rural surroundings. Dense urban areas also trap heat due to their inherent morphological characteristics. Heat retention is also aided by low turbulent mixing efficiency during the nighttime period [*Banta et al.*, 2007].

Another important factor that affects UHI is the anthropogenic heat released from buildings and vehicles. However, our simulation did not account for this as there is not yet a consistent method to enforce it within the numerical model for all the cities considered here. *Gutiérrez et al.* [2013], have previously considered

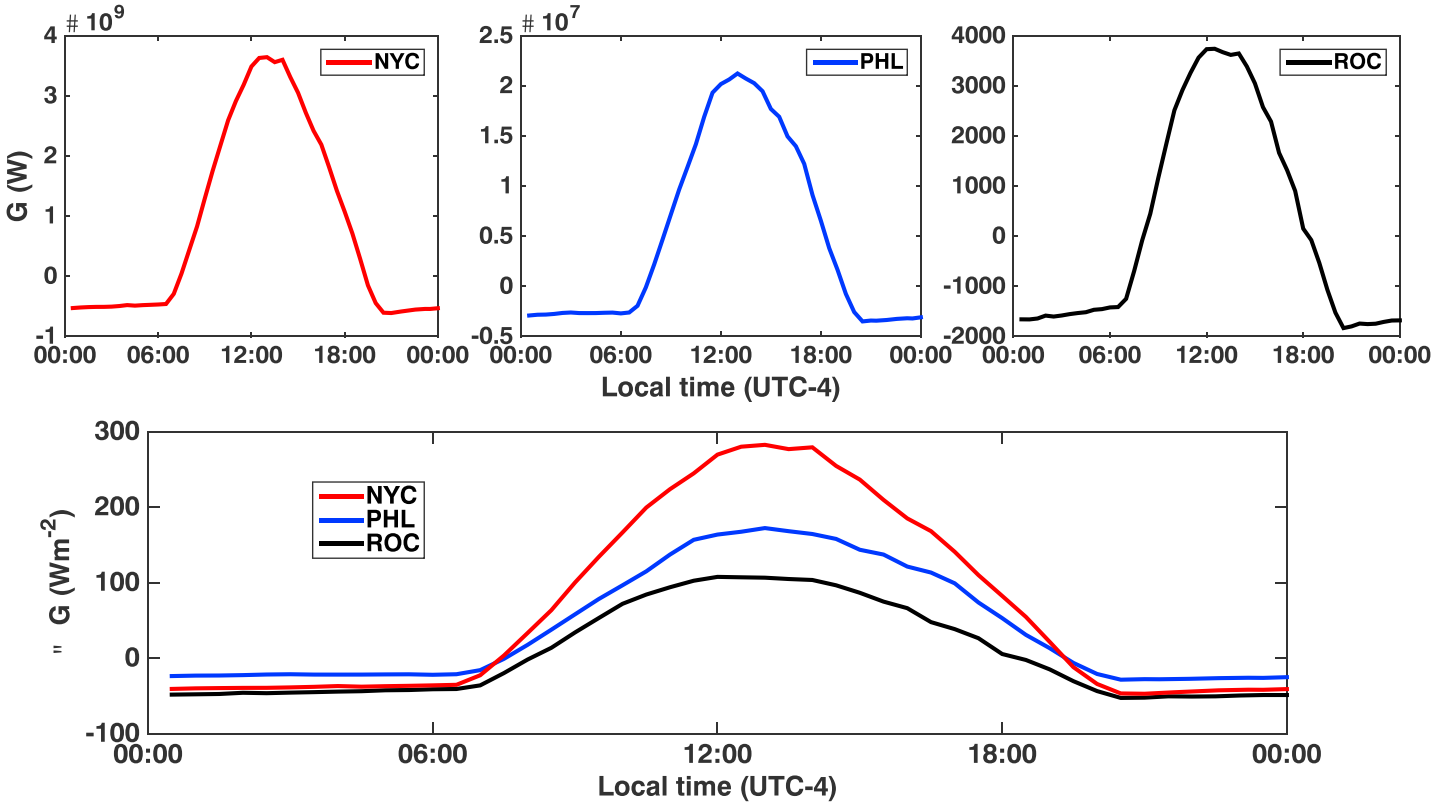


**Figure 5.** (top) The averaged spatially-aggregated storage heat flow for New York, Philadelphia, and Rochester. (bottom) Compares the variability in ensemble averaged storage heat flux. Positive flux is toward ground.

anthropogenic emissions for NYC by using a publicly available building database, but this data set is not yet uniformly available for all the urban areas. Moreover, aggregate inventories of fossil fuel use are seldom available at high spatial resolutions. If accounted for, the anthropogenic heat will play a nonnegligible role in altering the UHI.

### 3.2. UHI-Heatwave Interaction

Unlike UHIs, heat waves are synoptic-scale phenomena that can be described as persistent intensive hot periods that lead to severe human fatalities. Heatwaves are a result of sustained high pressure that brings hot air from the upper troposphere. During the simulation period, there were two heat wave episodes: one between 16 and 18 July and the other during 1–3 August. Our simulation results show (Figure 6) that heat waves generally exacerbate UHIs in upper tier cities, while in lower tier cities no significant amplification is detected. In NYC, Washington, and Baltimore, the overall UHI during heat wave episodes is higher, with the average UHI increasing by 1.5–2 K during the heat wave period. Here a heat wave is defined as any three consecutive days when the maximum temperature exceeds 32.2°C (90°F).

The amplification observed in the upper tier cities is far from consistent across the four cities. NYC experiences the largest UHI amplification of about 2 K occurring during the daytime; however, in Washington and Baltimore the nighttime UHI is amplified by 1.5–2 K, while the midday UHI remains almost unchanged. A test was performed to analyze the significance of this amplification. The null hypothesis, "no increase in UHI during heat waves," was disproved in all upper tier cities, while the lower tier cities were in agreement at 5% significance level. The probability of agreement with the null hypothesis was less than 1% for the upper tier cities. For Rochester, Harrisburg, and Bridgeport the probability was 10%, 74%, and 90%, respectively.

In NYC during the heat wave period, the wind direction in the afternoon hours switches to westerly. Figure 7 compares surface winds and 2 m air temperature in the afternoon (1430 local time) during a heat wave episode and a regular day. The wind barbs in the figure over NYC are predominantly from the west, and this is in

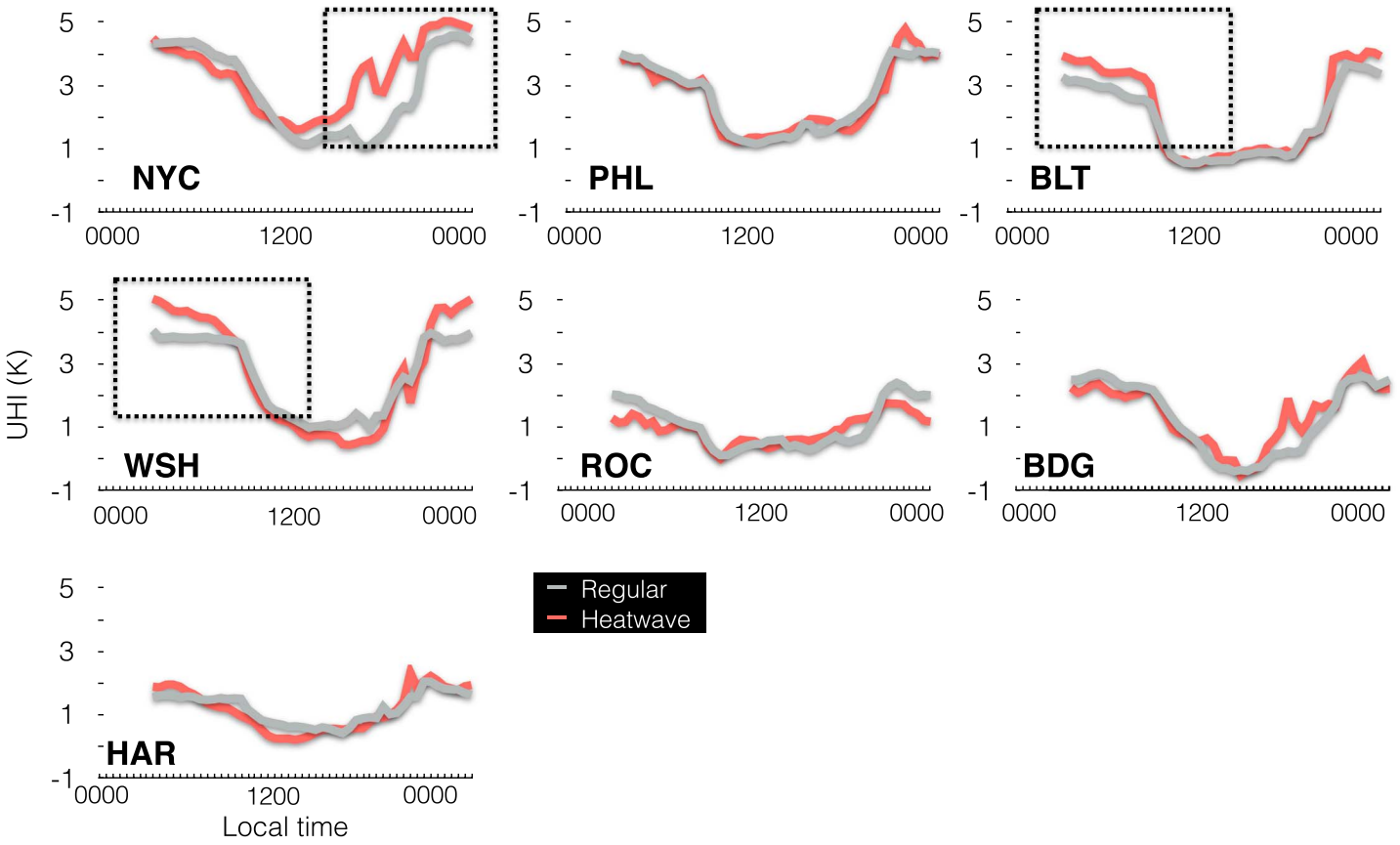


**Figure 6.** Comparing mean diurnal variability of UHI during heat wave episodes with UHI from non-heat-wave (regular) days. The heat wave days were 16–18 July and 1–3 August, and the rest were counted as regular days.

contrast to non-heat-wave days. In the summer months, NYC is cooled by southerly sea breeze; however, during the heat wave period, 90% of the winds are from the west. This loss in moderation of UHI by cool maritime air due to the switch in wind direction is the primary factor responsible for the amplification of UHI in NYC in the midafternoon hours during heat wave episodes. It should be noted that actual wind magnitudes could be different from the simulated results; this would be mainly due to the limitations in the urban land surface scheme in representing the complex urban geometry. Moreover, the land surface schemes use surface layer similarity theory, which is known to fail in dense urban environments [*Ramamurthy et al.*, 2015].

In Washington and Baltimore, the nighttime UHI rises by 1 K compared to non-heat-wave days; in Washington the UHI reaches a peak of 5 K at 0300 UTC. This amplification could be attributed to increased urban-rural soil moisture deficit. Figure 8 depicts the urban-rural soil moisture deficit for NYC, Washington, and Baltimore. The soil moisture deficit can be defined as follows:

$$\beta_D = \left(1 - \frac{\beta_u}{\beta_r}\right). \tag{2}$$

In the above equation, $\beta_D$ is the urban-rural relative soil moisture deficit and $\beta_u$ and $\beta_r$ are the urban and rural evaporative reduction factors defined as

$$\beta = \frac{\theta - \theta_w}{\theta_w - \theta_s}. \tag{3}$$

In equation (3), $\theta$ indicates volumetric soil moisture, $\theta_w$ and $\theta_s$ represent the wilting point and saturation point respectively. $\beta$ is the reduction factor that distinguishes actual evaporation from potential evaporation. It is clear from Figure 8 that during the second heat wave, the slope of the urban-rural moisture deficit for Washington and Baltimore is increasing rapidly. As the region is experiencing a severe dry down period,

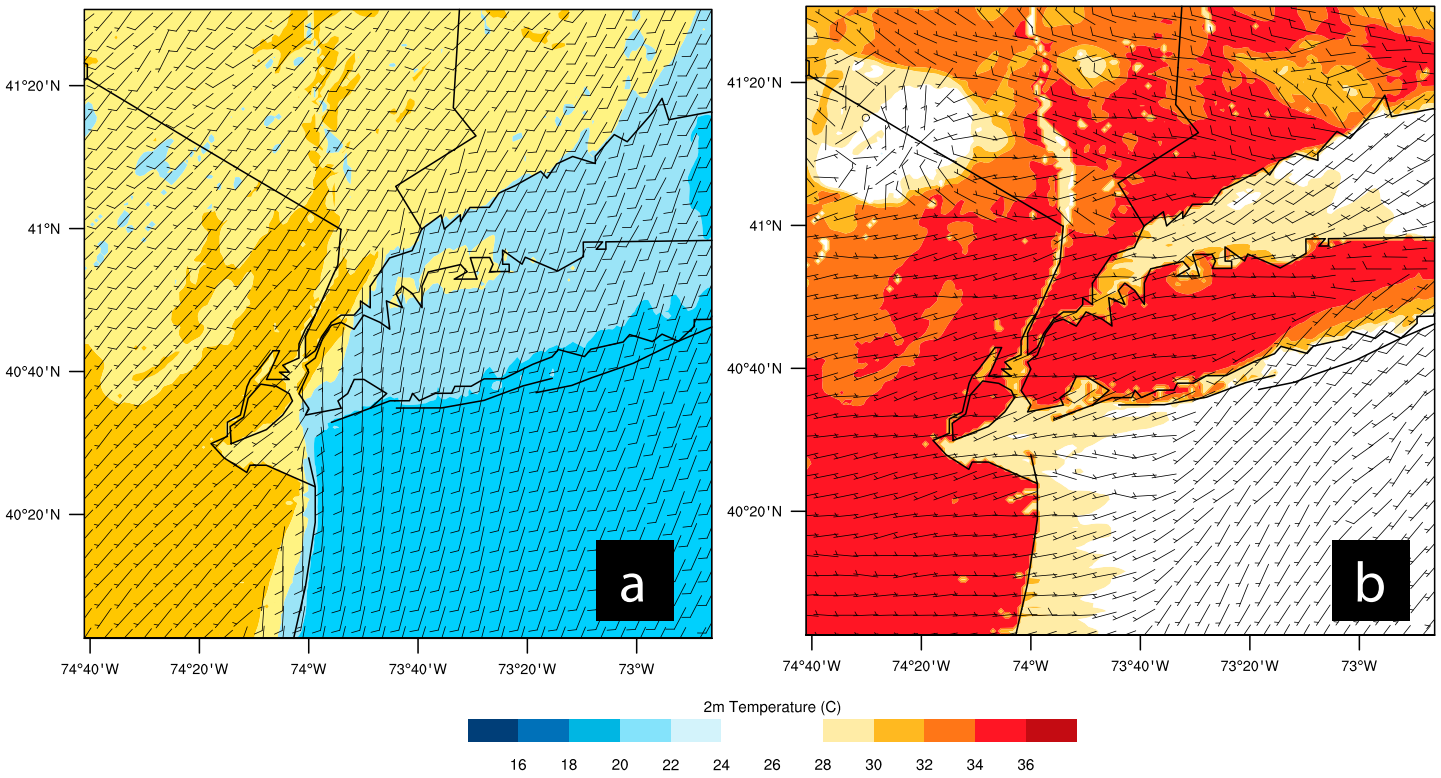


**Figure 7.** (a) The 10 m wind barbs superimposed on 2 m air temperature for a nonheat wave day (24 July 2006 at 1430 local time (1830 UTC)). (b) The same information but for a heat wave day (02 August 2006 at 1430 local time (1830 UTC)).

the moisture availability in the urban area is decreasing at a higher rate than the rural area. The increased temperature, deeper and drier boundary layer, and stronger convection all aid in pronounced desiccation of urban soil relative to rural soil during heat wave episodes. The average $\beta_D$ for Washington and Baltimore during the heat wave episode is twice compared to non-heat-wave days. This deficit in available moisture is most plausibly the cause for the amplification in UHI witnessed in Washington and Baltimore. In New York and Philadelphia, the $\beta_D$ values only increase marginally during this period, since they were already quite high (urban surfaces were already much drier that surrounding rural areas in these two cities). Thus, New York and Philadelphia experience greater urban-rural difference in moisture availability, even during regular days, due to the vast expanse of industrial and suburban land cover that surrounds them. This difference in available moisture between the urban core of New York and Philadelphia and their surrounding rural areas significantly influence their respective background UHIs but do not increase in impact during heat waves. In lower tier cities, due to the overall low thermal capacity and short urban-rural transect, the UHI remains unaltered during heat wave episodes.

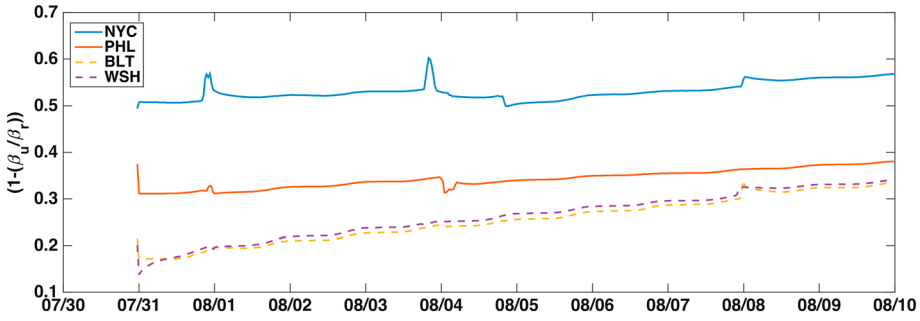


**Figure 8.** Soil moisture deficit for upper tier cities during the second half of the simulation. Baltimore and Washington exhibit higher rate of urban-rural deficit during the dry-down period.

The impact of soil moisture deficit on the overall urban climate is thus a key determinant of heat wave-UHI interaction that needs to be explored further. Urban soils, unlike natural ones, are highly disturbed. A patch of urban soil in a metropolitan area has typically been moved, graded, and/or or compacted over time [*Pavao-Zuckerman*, 2008]. Often as a result of construction and demolition activity at the site. Movement of soil and addition of nonnative soils are relatively common in developed areas. The contamination could inhibit surface soil moisture to seep in to deeper layers. While direct observation of soil moisture in urban areas is rare, the mosaic approach has enabled us to probe its dynamics better than previous modeling studies.

## 4. Conclusions

Our comparative analysis has confirmed that UHI development is highly complex and cannot be constrained or explained by simple binaries of urban and rural characteristics. While the amplitude of UHI is related to the physical size of the city, which is proportional to its thermal capacity, the UHI pattern, its variability and its interaction with heat waves are inherently linked to multiple dynamic factors such as secondary circulation and moisture availability. These results have also established that UHIs are highly localized. Despite the fundamental physics behind them being similar, they are strongly modulated by local dynamics. Philadelphia, for example, did not experience an exacerbation of the UHI during hear wave, unlike the other three top tier cities. This could be related to the urbanization pattern of the city that is more elongated along a Southwest-Northeast axis, compared to the circular pattern of the other cities, but further research is needed to confirm that hypothesis.

Heatwaves and their interaction with UHIs will have grave consequences for energy use and human health. The recently released International Panel on Climate Change report predicts the Northeastern U.S. to be highly vulnerable to extreme heat events [*Field and Van Aalst*, 2014]. The heat events are predicted to increase in intensity and occur more frequently [*Meehl*, 2004]. They result in high energy demand and during peak hours the increased demand stresses the power infrastructure leading to potential blackouts. In fact, power production itself can slow down during these periods, particularly wind power and hydroelectric power. It is known that a modest 1°C increase in air temperature over a midsized city will lead to 2% increase in electricity required for additional space cooling [*Akbari et al.*, 1992]. Heat will also impact human life. *Anderson and Bell* [2009] found that the human mortality rate jumped by 28% during a heat wave episode. Finally, the additional energy consumption will directly lead to an increase in greenhouse gas emissions.

To conclude, the WRF-MOSAIC-PUCM framework provides a cogent platform to study these local UHIs and their related impacts. Nevertheless, there are few areas that need further development and research:

1. Anthropogenic heat is one of the primary factors that affect UHI; however, there is not yet a consistent methodological platform to include this parameter in high-resolution simulations. Most energy use data sets are aggregated at city scale, which is too sparse and homogenizes consumption pattern at finer spatial scales. Hence, high-resolution maps of energy use pattern are necessary to close the urban surface energy balance in numerical schemes. Some efforts in that direction are underway [*Sailor et al.*, 2015] and can be helpful for future studies.
2. Our analysis has shown that upper tier cities have sharp gradients in surface soil moisture along the urban-suburban-rural transect. This soil moisture deficit has a profound impact on the UHI at the local scale as lack of soil moisture leads to incoming radiation being disproportionately partitioned to sensible heat. In large metropolitan centers the characteristic length scale of this deficit will be on the orders of several kilometers, which could have potential ramifications to regional climate. However, very few studies have been conducted to understand the soil state and properties in urban areas. Urban soils are highly disturbed compared to natural soils, and this leads to variability in their hydrological and and thermal characteristics. More work is needed on this topic in order to more accurately represent urban soils in high-resolutions numerical simulations.

The proposed additions will have a significant impact on urban-scale numerical simulations and are vital to understanding long-term trends and characterizing the impact of UHI and heat waves.

**Acknowledgments**
The work was partly supported by the Department of Defense Army Research Office under grant W911NF-15-1-0526 and by the US National Science Foundation's Sustainability Research Network Cooperative Agreement 1444758. The simulations were performed on Yellowstone super computer at the National Center For atmospheric research (P36861020). Both the data and input files necessary to reproduce the experiments with WRF are available from the authors upon request. It will be made available in the PI's webserver at ufo.ccny.cuny.edu.

## References

Akbari, H., S. Davis, and S. Dorsano (1992), *Cooling Our Communities: A Guidebook on Tree Planting and Light-Colored US Environmental Protection Agency*, Climate Change Division.

Allwine, K. J., J. H. Shinn, G. E. Streit, K. L. Clawson, and M. Brown (2002), Overview of URBAN 2000: A multiscale field study of dispersion through an urban environment, *Am. Meteorol. Soc.*, *83*, 521–536.
Anderson, B. G., and M. L. Bell (2009), Weather-related mortality: How heat, cold, and heat waves affect mortality in the United States, *Epidemiology*, *20*, 205–213, doi:10.1097/EDE.0b013e318190ee08.
Arnfield, A. J. (2003), Two decades of urban climate research: A review of turbulence, exchanges of energy and water, and the urban heat island, *Int. J. Climatol.*, *23*(1), 1–26.
Banta, R. B., L. Mahrt, D. Vickers, J. Sun, B. Balsley, Y. L. Pichugina, and E. Williams (2007), The very stable boundary layer on nights with weak low-level jets, *J. Atmos. Sci.*, *64*, 3068–3090, doi:10.1175/JAS4002.1.
Black, E., M. Blackburn, G. Harrison, B. Hoskins, and J. Methven (2004), Factors contributing to the summer 2003 European heatwave, *Weather*, *59*(8), 217–223.
Chen, F., and Y. Zhang (2009), On the coupling strength between the land surface and the atmosphere: From viewpoint of surface exchange coefficients, *Geophys. Res. Lett.*, *36*, L10404, doi:10.1029/2009GL037980.
Chen, X. L., H. M. Zhao, P. X. Li, and Z. Y. Yin (2006), Remote sensing image-based analysis of the relationship between urban heat island and land use/cover changes, *Remote Sens. Environ.*, *104*, 133–146.
Cui, L., and J. Shi (2012), Urbanization and its environmental effects in Shanghai, China, *Urban Climate*, *2*, 1–15.
Department of Health NYC (2006), NYC vital signs: Investigative report *Prepared by Department of Health and Mental Hygiene*.
Dudhia, J. (1989), Numerical study of convection observed during the winter monsoon experiment using a mesoscale two-dimensional model, *J. Atmos. Sci.*, *46*(20), 3077–3107.
Field, C., and M. Van Aalst (2014), Climate change 2014: Impacts, adaptation, and vulnerability. 1 *Intergovernmental Panel on Climate Change Report*.
Gedzelman, S. D., S. Austin, R. Cermak, N. Stefano, S. Patridge, S. Queensberry, and D. A. Robinson (2003), Mesoscale aspects of the urban heat island around New York City, *Theor. Appl. Climatol.*, *75*, 29–42.
Grimmond, C. S. B., et al. (2006), Progress in measuring and observing the urban atmosphere, *Theor. Appl. Meteorol.*, *84*(1), 3–22.
Grimmond, C. S. B., et al. (2010), Climate and more sustainable cities: Climate information for improved planning and management of cities (producers/capabilities perspective), *Procedia Environ. Sci.*, *1*, 247–274.
Gutiérrez, E., et al. (2013), a new modeling approach to forecast building energy demands during extreme heat events in complex cities, *J. Sol. Energy Eng.*, *135*(4040906).
Haeger-Eugensson, M., and B. Holmer (1999), Advection caused by the urban heat island circulation as a regulating factor on the nocturnal urban heat island, *Int. J. Climatol.*, *19*, 975–988.
Kanda, M. (2007), Progress in urban meteorology: A review, *J. Meteorol. Soc. Jpn.*, *85*, 363–383.
Li, D., and E. Bou-Zeid (2013), Synergistic interactions between urban heat islands and heat waves: The impact in cities is larger than the sum of its parts, *J. Appl. Meteorol. Climatol.*, *52*(9), 2051–2064.
Li, D., and E. Bou-Zeid (2014), Quality and sensitivity of high-resolution numerical simulation of urban heat islands, *Environ. Res. Lett.*, *9*(5055001).
Li, D., E. Bou-Zeid, F. Chen, and J. Smith (2013), Development and evaluation of a mosaic approach in the WRF-Noah framework, *J. Geophys. Res. Atmos.*, *118*, 11,918–11,935, doi:10.1002/2013JD020657.
Meehl, G. A. (2004), More intense, more frequent, and longer lasting heat waves in the 21st century, *Science*, *305*(5686), 994–997, doi:10.1126/science.1098704.
Meir, T., P. Orton, J. Pullen, T. Holt, W. Thompson, and M. Arend (2013), Forecasting the New York City urban heat island and sea breeze during extreme heat events, *Weather Forecast.*, *28*(6), 1460–1477.
Mellor, G. L., and T. Yamada (1974), A hierarchy of turbulence closure models for planetary boundary layers, *J. Atmos. Sci.*, *31*(7), 1791–1806.
Mlawer, E. J., S. Taubman, P. Brown, M. Iacona, and S. Clough (1997), Radiative transfer for inhomogeneous atmospheres: RRTM, a validated correlated-k model for the longwave, *J. Geophys. Res.*, *102*(D1416663), doi:10.1029/97JD00237.
Oke, T. R. (1982), The energetic basis of the urban heat island, *Q. J. Roy. Meteorol. Soc.*, *108*(455), 1–24.
Pavao-Zuckerman, M. A. (2008), The nature of urban soils and their role in ecological restoration in cities, *Restor. Ecol.*, *16*(4), 642–649.
Ramamurthy, P., E. Bou-Zeid, Z. Wang, M. Baeck, J. Smith, J. Hom, and N. Saliendra (2014), Influence of sub-facet heterogeneity and material properties on the urban surface energy budget, *J. Appl. Meteorol. Climatol.*, *53*(9140331150345000–2129).
Ramamurthy, P., D. Li, and E. Bou-Zeid (2015), High-resolution simulation of heatwave events in New York City, *Theor. Appl. Climatol.*, 1–14, doi:10.1007/s00704-015-1703-8.
Rotach, M. W., R. Vogt, and C. Bernhofer (2005), BUBBLE—a major effort in urban boundary layer meteorology, *Theor. Appl. Climatol.*, *81*, 231–261.
Rosenzweig, C., et al. (2009), Mitigating New York City's heat island: Integrating stakeholder perspectives and scientific evaluation, *Bull. Am. Meteorol. Soc.*, *90*(9), 1297–1312.
Sailor, D. J. (2008), A green roof model for building energy simulation programs, *Energ. Buildings*, *40*(8), 1466–1478.
Sailor, D. J., M. Georgescu, J. M. Milne, and M. A. Hart (2015), Development of a national anthropogenic heating database with an extrapolation for international cities, *Atmos. Environ.*, *118*, 7–18.
Taha, H. (1997), Urban climates and heat islands: Albedo, evapotranspiration, and anthropogenic heat, *Energ. Buildings*, *25*(2), 99–103.
Vahmani, P., and G. A. Ban-Weiss (2016), Impact of remotely sensed albedo and vegetation fraction on simulation of urban climate in WRF-urban canopy model: A case study of the urban heat island in Los Angeles, *J. Geophys. Res. Atmos.*, *121*, 1511–1531, doi:10.1002/2015JD023718.
Wang, Z., E. Bou-Zeid, and J. A. Smith (2013), A coupled energy transport and hydrological model for urban canopies evaluated using a wireless sensor network, *Q. J. Roy. Meteorol. Soc.*, *139*(675), 1643–1657, doi:10.1002/qj.2032.
Wickam, J., S. Stehman, L. Gass, J. Dewitz, J. Fry, and T. Wade (2013), Accuracy assessment of NLCD 2006 land cover and impervious surface, *Remote Sens. Environ.*, *130*, 294–304.
Xoplaki, E., J. F. Gonzales-Ruoco, J. Lauterbacher, and H. Wanner (2003), Mediterranean summer air temperature variability and its connection to the large-scale atmospheric circulation and SSTs, *Climate Dynam.*, *20*(7-8), 723–739.